Virtual-Flux Finite Control Set Model Predictive Control of Switched Reluctance Motor Drives

Diego F. Valencia*, Silvio Rotilli Filho*, Alan Dorneles Callegaro*, Matthias Preindl† and Ali Emadi*
*McMaster Automotive Resource Center
McMaster University, Hamilton, ON L8S4L8, Canada
Email: valend1@mcmaster.ca
†Department of Electrical Engineering
Columbia University, New York City, NY, USA

***Abstract*—In this paper, a virtual-flux finite control set model predictive control (FCS-MPC) strategy of switched reluctance motor (SRM) drives is proposed. This technique uses a flux linkage-tracking algorithm to indirectly control the phase current. The algorithm is based on an estimated virtual flux obtained from the static characteristics of the machine. A cost function is used to evaluate the switching state that produces the minimum error. A state graph for switching states limitation is also proposed to reduce the number of commutations and computational burden. Simulation results evidence the enhanced performance of the proposed technique with respect to hysteresis control for current tracking using two different current shaping techniques: torque sharing function (TSF) and radial force shaping (RFS).**

***Index Terms*—Finite Control Set Model Predictive Control (FCS-MPC), Hysteresis Current Control, Switched Reluctance Motor, Virtual-Flux Control.**

I. Introduction

Switched reluctance machines (SRM) have been receiving increasing attention for traction applications as they present significant advantages with respect to induction and permanent magnet machines (PMSM) [1]. Their structure has a simple, low-cost and robust design allowing a more reliable high-speed and high-temperature operation [2]. Although their inherent torque ripple and acoustic noise have limited the market attractive of SRM drives, these issues can be minimized by a proper machine design [3] and control strategies.

In terms of control, torque ripple can be reduced by the strategical distribution of the produced torque between individual phase components. These components compensate each other during the phase transient to guarantee a constant torque; this technique is known as the torque sharing function (TSF) [4]. Similarly, the acoustic noise can be mitigated by minimizing the radial force ripple using phase current shaping [5]. This can also be used to decrease the temporal harmonic content of the most critical spatial orders, thus reducing the vibration mode excitation. This technique is known as radial force shaping (RFS) [6]. In both cases, the control approach defines particular profiling of the phase currents and sets the references as a function of the rotor position, reducing the problem to a reference current tracking task.

The problem of current tracking in SRM has been conventionally addressed by the use of hysteresis current controllers (HCC). This is a simple and fast technique with the main disadvantages of a variable switching frequency and high current ripple [7]. In addition, it is required to know the phase conduction angles, which needs detailed knowledge about the speed and reference current. Alternatively, the use of proportional-integral (PI) controllers with pulse width modulation (PWM) generation offers a constant switching frequency, but the compensator parameters are difficult to tune due to the nonlinear characteristics of the plant [8]. In addition, PI controllers provide a limited dynamic response, which is required for the torque and force control given the non-conventional shapes of the reference currents. Other control techniques such as sliding mode control [10], online auto-tuning loops [11], [12] or linearized models for PWM performance improvement [13] have been also investigated.

Model predictive control (MPC) is a promising technique for nonlinear systems which uses a model to predict the future behavior of the plant. This uses a cost function to select the control action, thus solving the optimal control problem per sampling period. This is especially applied to constrained finite-time processes. This method has been successfully applied to electrical drives, overcoming the fast sampling rate requirements with modern processors [14]. In fact, recent trends have shown a growth in the use and application of MPC for high-performance AC drives such as induction or permanent magnet motors [15].

In the case of SRM drives, different predictive control approaches have been considered to address the current tracking problem. Examples include modulator-based techniques such as deadbeat [16] and generalized predictive control (GPC) [17], or non-modulator-based ones like hysteresis predictive control [18]. They are classified as 'predictive' because they predict the future system behavior, then selecting the control action based on this [19]. Furthermore, if a cost function minimization is used to select the control action, the method is considered as MPC, which is based on either a finite control set (FCS-MPC) or a continuous control set (CCS-MPC).

The selection of either CCS-MPC or FCS-MPC depends on the application as they have different control properties. Differences are related to the current ripple of the power converter and getting either a constant or variable switching frequency. In general, CCS-MPC has been used for current control considering advanced features such as online inductance calibration [20], but FCS-MPC has not been fully explored for current tracking in SRM drives. From its applications in AC drives, the advantages of FCS-MPC in terms of dynamic response and the consideration of nonlinear constraints are evident [21].

In addition, the use of FCS-MPC allows the adaptation of the virtual-flux concept, initially introduced for PMSM drives [22]. This concept allows linearizing the MPC problem using static flux maps that transform the nonlinear current control problem into a linear virtual flux control problem. In PMSM, this is important to deal with saturation and other non-ideal behavior. Therefore, it results in a useful technique for the SRM highly nonlinear characteristics.

In this paper, a virtual-flux FCS-MPC strategy for current tracking in SRM is proposed. The technique predicts a virtual-flux based on a discrete voltage equation and evaluates the switching state that produces the minimum error with respect to the flux reference. The reference and the actual flux are obtained through the offline static characteristics of the machine. Simulation results comparing the effectiveness of the method with respect to conventional soft-switching and hard-switching HCC are provided for reference current tracking using torque sharing function and radial force shaping algorithms.

II. Fundamentals of SRM drives

A. Electromagnetic model

The SRM operation is based on the sequential excitation of different windings to generate flux paths along unaligned stator and rotor poles, thus generating a magneto-motive force, which makes the poles moving towards an aligned position. One of the main advantages for operation and modeling of these machines is the possibility to operate the phases independently. The phase voltage equation of the SRM, by neglecting mutual coupling between phases, can be expressed by (1):

$$v_{ph} = i_{ph} R_{ph} + \frac{d\psi_{ph}}{dt} \tag{1}$$

where v_{ph}, i_{ph}, R_{ph} and ψ_{ph} are the terminal voltage, current, resistance and phase flux linkage, respectively.

In order to obtain an optimal operation, this type of motor has to work in the saturation region; therefore, the magnetic characteristic is highly non-linear, and the flux linkage per phase ψ_{ph} is a nonlinear function of the phase current i_{ph} and the electric angle per phase θ_{ph}. Fig. 1 shows the flux linkage characteristic for a 5 kW four-phase 8/6 SRM obtained by FEA, which is used as a reference machine for this work.

The relation between the phase electrical angle and the mechanical rotor position is defined by the number of stator and rotor poles. If a stator pole is positioned in between two consecutive rotor poles is zero electrical degrees (unaligned position), an electrical cycle is completed when the rotor moves and the stator pole reaches the next unaligned position.

By inspecting (1) and Fig. 1 it can be concluded that the operation of each phase in between 180° and 360° electrical, makes the machine operate in generating mode as the rate of change of the flux linkage is negative.

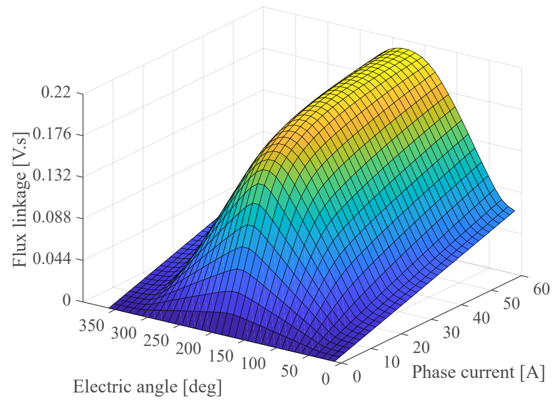

Fig. 1. Flux linkage static characteristic of a four-phase 8/6 SRM

B. Power converter model

The asymmetric half-bridge converter shown in Fig. 2(a) is commonly used for SRM drives as it allows to take advantage of the independent operation of the phases. Fig. 2(a) shows the topology for the control of two phases, which is repeated if more phases are required. The states of the SRM are represented by the operation of the inverter. In state 1, as shown in Fig. 2(b), the correspondent phase is energized with V_{dc} by activating both switching devices s_{j1} and s_{j2}, with j being the active phase. In this state, the phase current is increased just limited by the back-EMF at higher speeds. The state 0 is called the freewheeling mode, in which the current stored in the phase inductance is allowed to circulate within one of the inverter loops, using the conduction of the diode D_{j1} and s_{j2}, as shown in Fig. 2(c). The Fig. 2(d) illustrates state -1, in which both switching devices are off, and the previously stored phase current circulates through the diodes. In this state, the phase is energized with $-V_{dc}$ from the source. This state is commonly used when the phase has to be deactivated faster or for regenerative operation. It is worth noticing that the phase current in SRM always maintains the same direction independent of the operating condition.

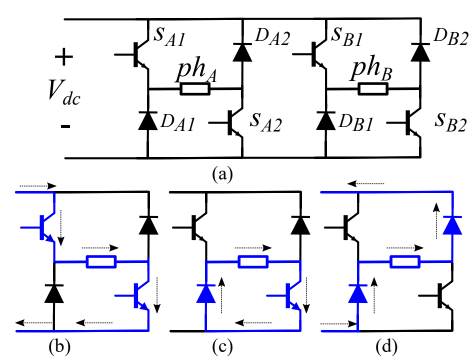

Fig. 2. (a) Asymmetric half-bridge converter topology (b) State "1" with $S_{j1} = 1, S_{j2} = 1$ (c) State "0" with $S_{j1} = 0, S_{j2} = 1$ (d) State "-1" with $S_{j1} = 0, S_{j2} = 0$

C. Hysteresis current control

The HCC has been conventionally used for SRM due to its simple digital implementation and control rule. It defines an upper and lower band (I_{up} and I_{lo}) around the reference current value to act as boundaries for the instantaneous phase current. Depending on the operating mode, each phase should only conduct current in between the corresponding conduction angles, $0° - 180°$ for motoring mode and $180° - 360°$ for generating mode. If the correspondent electrical angle for phase j is within the operating region, the conduction signal G_j is active, and the logic in (2) is followed.

$$v_{ph}\left(k\right) = \begin{cases} 0 & G_j \leq 0 \text{ and } i_{ph} = 0 \\ -V_{dc} & G_j \leq 0 \text{ and } i_{ph} > 0 \\ v_{ctrl} & G_j > 0 \text{ and } i_{ph} \geq I_{up} \\ +V_{dc} & G_j > 0 \text{ and } i_{ph} < I_{lo} \\ v_{ph}\left(k-1\right) & G_j > 0 \text{ and } I_{up} > i_{ph} \geq I_{lo} \\ 0 & Otherwise \end{cases} \tag{2}$$

where v_{ctrl} depends on the operating mode. For soft-switching (SS) mode, the freewheeling or 0 state of the inverter is used to let the current reduce by circulating within the inverter; therefore $v_{ctrl} = 0$. In hard-switching (HS) operation, the current is forced to decrease by applying a negative voltage, the freewheeling mode is not considered, and only states 1 and -1 are used to regulate the current, making $v_{ctrl} = -V_{dc}$.

The use of either HCC-SS or HCC-HS depends on the hardware characteristics. SS mode guarantees lower switching losses but increases the thermal stress in one of the switching devices under freewheeling mode, due to higher conduction losses. On the other hand, the use of HS produces the opposite effect plus possible dv/dt due to the higher voltage step.

III. Proposed Virtual-Flux FCS-MPC Strategy

Fig. 3 shows the block diagram of the proposed virtual-flux FCS-MPC of SRM drive. The execution of the proposed algorithm works as follows. First, the current and rotor position are measured at the instant $k-1$. After delay compensation to get the flux at (k), the possible future plant states are predicted for the next sampling periods, with a horizon of 1 step, which means, for the sampling period $k+1$. The predicted states are compared to the reference flux and evaluated with a cost function. The one with the lowest cost is used as a plant input in the next sampling period.

It is worth noticing that this technique is, in reality, an indirect current tracking algorithm. Although it uses a flux-based model to describe the system in a simple way, the stator flux cannot be measured in conventional drives; therefore, a virtual flux is calculated and used as a state variable. This flux is determined based on static flux maps as the one in Fig. 1. Therefore, the measurements of current i_{ph} and rotor position θ_{ph} allow obtaining the flux ψ_{ph}. The same transformation is applied to the reference currents, thus making the system to behave as a current controller. The advantage of the virtual-flux domain is the independence of the closed-loop behavior of the machine type, as the current-flux map is external. Hence,

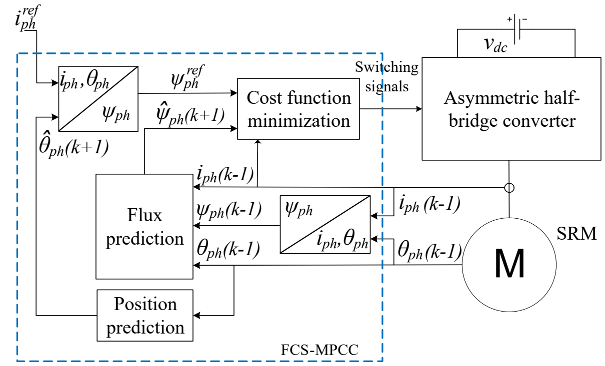

Fig. 3. Block diagram of the proposed virtual-flux FCS-MPC technique

simple stability and robustness can measure, which give also computational benefits especially if longer horizons are used [23].

A. Discrete dynamic model, state prediction and runtime compensation

The state prediction of the proposed technique is based on the discretized phase voltage equation in (1) considering the forward Euler approximation as:

$$\hat{\psi}_{ph}(k+1) = \psi_{ph}\left(k\right) + T_s\left(v_{ph}^g - i_{ph}\left(k\right)R_{ph}\right) \tag{3}$$

where T_s is the discrete control period and R_{ph}, i_{ph} and ψ_{ph} are the phase resistance, current and flux linkage. The applied terminal voltage v_{ph}^g represents all possible discrete switching states of the inverter. Unlike conventional AC drives, this value can be independently evaluated per each phase, thus giving only three possible voltage values to be applied by using an asymmetric converter: V_{dc}, 0 or $-V_{dc}$.

In practice, the calculated voltage is not set instantaneously after the measurements, but after the calculations in the algorithm; therefore, delay compensation is applied. Considering the convention in which measurements are taken at the sampling period $k-1$, the delay compensated flux $\psi_{ph}(k)$ can be determined by:

$$\psi_{ph}(k) = \psi_{ph}(k-1) + T_s(v_{ph}(k-1) - i_{ph}(k-1)R_{ph}) \tag{4}$$

where $v_{ph}(k-1)$ is stored from the previous control action calculation, and the value $\psi_{ph}(k-1)$ is obtained by the static flux map using the measured phase current $i_{ph}\left(k-1\right)$ and the electric angle $\theta_{ph}(k-1)$. The flux map in Fig. 1 is inverted and the values of $\psi_{ph}(k)$ and $\theta_{ph}(k)$ are used as input to obtain the delay compensated current $i_{ph}(k)$. This current is then used to compute the predicted flux $\hat{\psi}_{ph}(k+1)$ in (3). The compensated electrical angle is calculated using (5) and assuming constant speed with respect to the sampling period.

$$\theta_{ph}\left(k\right) = \theta_{ph}\left(k-1\right) + T_s\omega_r\left(k-1\right) \tag{5}$$

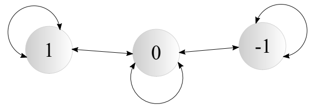

Fig. 4. Switch state graph with possible state transitions per each phase

B. State limitations

The number of possible discrete states that are considered for the prediction in the next sampling period can be limited as a function of the present state. Fig. 4 presents a simple phase switch state graph to limit the v_{ph}^{g} inputs of the predicted flux linkage in (3). Several benefits can be obtained from such a limitation graph. Initially, the number of predictions and equations in the cost function are reduced, improving the computational burden. As the application of v_{ph}^{g} with opposite polarity is now restricted, the operation leads to a better dv/dt behavior as well as a lower current ripple. Finally, as the transition from state 1 to state -1 requires the simultaneous switching of two devices s_{j1} and s_{j2} (See Fig. 2), forcing an intermediate state 0 limits the switch state changes to only one per sampling period, reducing the switching frequency [24].

C. Cost function

The cost function is the stage where the voltage to be applied in the next sampling time is decided. For each possible switching state, the cost is calculated, and the one producing the lowest cost is selected. Since the proposed controller is based on the virtual-flux tracking, a cost function using the phase flux linkage is proposed in (6). First, the reference current is transformed into a reference flux based on the flux maps like the one in Fig. 1. The electrical angle used for this transformation has to be considered at the same sampling period than the predicted phase flux; this is at the instant $k+1$. To compute $\theta(k+1)$ the same expression (5) is adapted.

$$\min G_1 = \left|\hat{\psi}_{ph}^{ref} - \hat{\psi}_{ph}^{v_g}\left(k+1\right)\right|^2 \tag{6}$$

D. Control limitations

Drives thermal constraints are commonly associated with a maximum absolute current. As the proposed technique does not directly regulate the current, additional considerations must be defined for the maximum current limitation. The idea is to prevent a control action that causes a current larger than the maximum current i_{max}. For this, a limitation term I_m is added to the cost function as defined in (7):

$$I_m\left(k+1\right) = \begin{cases} 0 & \left|\hat{i}_{ph}\left(k+1\right)\right| \leq \left|i_{max}\right| \\ \delta \gg 0 & \left|\hat{i}_{ph}\left(k+1\right)\right| > \left|i_{max}\right| \end{cases} \tag{7}$$

The cost function is then modified to include the limitation term as (8). The value of I_m depends on the predicted phase current. If the current is predicted to go beyond the limit, the value of I_m will make the cost to be the highest possible number, thus preventing that switching state to be applied.

$$\min G = \left|\hat{\psi}_{ph}^{ref} - \hat{\psi}_{ph}^{v_g}\left(k+1\right)\right|^2 + I_m\left(k+1\right) \tag{8}$$

IV. Simulation Results

The simulation results were obtained based on a 5 kW, four-phase 8/6 SRM drive with flux linkage characteristics shown in Fig. 1. The motor was driven by an asymmetric converter with 300 V dc-link voltage. It is assumed that the SRM drive is operated in torque control mode while driven by a dyno, guaranteeing a constant speed. Although in practice the dyno would not be able to avoid speed fluctuations due to the torque transients or the SRM inherent torque ripple at low speed, it is assumed smooth speed transition for simulation results. To produce the reference currents, two different current shaping techniques were used, TSF and RFS. Given a reference current, the steady state and dynamic response were evaluated and compared to the benchmark technique, HCC operating in both soft-switching and hard-switching modes. The sampling interval was set to $f_{samp} = 50$ kHz so that a maximum switching frequency of 50 kHz results. The simulation considers the transient response for variations in the speed and torque commands.

A. Reference generation procedure

The reference currents are based on two current shaping techniques for torque ripple and acoustic noise reduction, torque sharing function and radial force shaping, respectively.

The TSF reduces the torque ripple by minimizing the torque dips caused by the phase commutation. It guarantees that the sum of the individual phase torque contributions is equal to the commanded torque. The commutation between one phase and the next one can be done using different approaches such a linear, quadratic or cubic reference. The distribution of the phase torque between the independent phases can also be optimized, considering the dynamics of the machine itself. Further information TSF and its optimization can be found on [4]. In this paper, a simple cubic TSF is considered.

In the case of RFS, an offline multi-objective optimization process shapes the phase current to produce an equivalent Gaussian-shaped radial force and to reduce the torque ripple. These waveforms are stored in a 2D-look-up table (LUT) and are defined as a function of the torque and electrical angle. This LUT is then used to obtain the current reference based on a torque reference and the information of the electrical angle. The detailed process on the current shaping for acoustic noise reduction can be found on [6].

B. Results and analysis

Figs. 5(a) to 5(c) show the performance of the proposed and benchmark controllers for the RFS-based references, while Figs. 5(d) to 5(f) show the correspondent results for TSF algorithms. Only the currents of phases A and B are shown for simplicity in the visualization. For both cases, an initial speed of 500rpm with a torque of 1N.m were set. The speed was then increased to 1000rpm with a slope limitation of 900rpm/s, thus emulating the real dynamics of a accelerating dyno machine. Next, torque command is changed to 6N.m. Finally, under the same load, a speed reversal to -1000rpm with the same speed ramp limitation was applied, thus making the machine

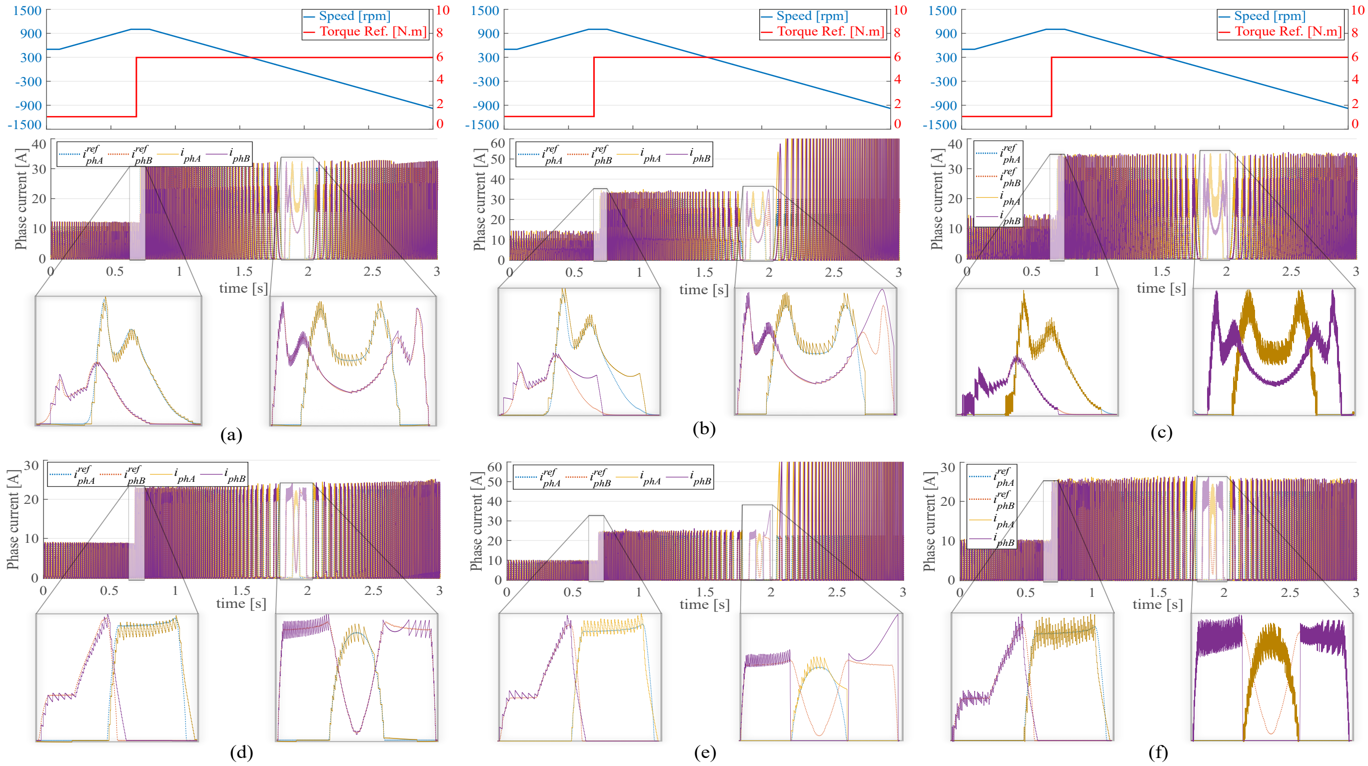

Fig. 5. Dynamic response to changes in load and dyno speed. (a) RFS reference tracked by MPC (b) RFS reference tracked by HCC-SS (c) RFS reference tracked by HCC-HS (d) TSF reference tracked by MPC (e) TSF reference tracked by HCC-SS (f) TSF reference tracked by HCC-HS

to operate in generating mode. The use of negative speeds and the generating mode is not commonly reported in SRM testing because it requires a change in the phase excitation sequence. Also, as the equivalent to the field current is generated from the stator currents, it is necessary to keep certain excitation before operating in the generating region of Fig. 1.

The TSF-based reference currents have a slow transient during the current growing up and down, followed by an approximately constant value, shaping a trapezoidal-wise waveform. The proposed technique in Fig. 5(d) evidences a satisfactory tracking in all the operating conditions. It suffers a delay during the outgoing current of the turning-off phases, but this phenomenon is related to the machine limitations in terms of the maximum rate of change of flux linkage. This can be solved by offline optimization techniques [25]. The response for HCC-SS is shown in Fig. 5(e). The dynamic response to the torque step offers better average tracking as the conduction angles are synchronized with the TSF conduction angles; however, for speed reversal, this method loses tracking as the electrical angle oscillates outside the activation interval. In addition, HCC-SS cannot operate in generating mode for current tracking as the 0 state keeps the current flowing due to the back-EMF. Therefore, the current tends to keep increasing. On the other hand, HCC-HS offers good tracking but increases the current ripple and commutations. It is also limited by the conduction angles interval in the speed reversal.

The current waveform from RFS technique does not present a region of constant value, providing a dynamic change of current as a function of the rotor position. Fig. 5(a) shows the response of the proposed technique, with a major tracking error at the beginning of the curve. This error is explained by the flux characteristic in Fig. 1. For small θ_e, the rate of change of flux linkage is low, which represents a small inductance; therefore, for small variations in the terminal voltage, high changes in the phase current are obtained, making more difficult the control, especially for high power machines. In this model, however, the proposed technique can be adapted without additional constraints. In the case of HCC-SS in Fig. 5(b), the same problem is evidenced around the unaligned position, but only two states are considered during the conduction interval and the dynamics is slower. This is more noticeable around the aligned position. As the θ_e is still in the conduction interval, the conduction signal G_j remains active, and the current is slowly reduced by freewheeling operation; however, it cannot be reduced as fast as the reference current due to the higher inductance at aligned position. Finally, in the case of HCC-HS, the reference current is successfully tracked, but the current ripple increases.

To compare the performance of the algorithms, the rms error and the maximum average switching frequency per operating point of RFS are shown in Table I. The switching frequency is estimated per switching device and considering the number of commutations within a time window of 1 ms. It can be seen how the proposed technique offers more accurate results with a reduced switching frequency for all operating points.

TABLE I
ESTIMATED RMS ERROR AND AVERAGE SWITCHING FREQUENCY

Operating point	$\epsilon_{rms}(A)$			$f_{sw}^{av}(kHz)$		
	MPC	HCC-SS	HCC-HS	MPC	HCC-SS	HCC-HS
$T_{ref} = 1Nm$ $\omega = 500rpm$	0.5323	1.6867	1.1257	3	5	5.5
$T_{ref} = 1Nm$ $\omega = 1000rpm$	0.5844	1.8373	1.1217	3	5.5	5
$T_{ref} = 6Nm$ $\omega = 1000rpm$	1.0324	2.8234	1.3298	6	9.5	6
$T_{ref} = 6Nm$ $\omega = -1000rpm$	1.0116	N/A	1.3340	5	N/A	8

V. CONCLUSION

A virtual-flux FCS-MPC method for the SRM drives has been developed. The control is based on a virtual-flux tracking algortihm which predicts the phase flux linkage using the machine voltage equation and flux static characteristics. A cost function is then used to evaluate the switching states that produce the lowest flux linkage error with respect to a flux reference. A state limitation graph was also proposed to limit the number of commutations and computational burden. This controller indirectly tracks the provided phase current.

Simulation results evidenced the improved performance of the proposed technique with respect to the benchmark HCC methods. For this, two current shaping strategies were used: TSF, with trapezoidal-wise waveforms, and RFS, with more dynamically challenging waveforms. It was found that the HCC methods presents drawbacks related to different operating points, while the proposed technique can work consistently through all of them. The main benefits of the proposed method are: the current tracking accuracy is improved, and the estimated switching frequency is lower. Moreover, the FCS-MPC can operate in the four quadrants tracking current even for generating mode.

ACKNOWLEDGMENT

This research was undertaken, in part, thanks to funding from the Canada Excellence Research Chairs (CERC) Program.

REFERENCES

[1] J. W. Jiang, B. Bilgin, and A. Emadi, "Three-Phase 24/16 Switched Reluctance Machine for a Hybrid Electric Powertrain," *IEEE Transactions on Transportation Electrification*, vol. 3, no. 1, pp. 76–85, Mar. 2017.

[2] B. Bilgin, J. W. Jiang, and A. Emadi, *Switched Reluctance Motor Drives: Fundamentals to Applications*. Taylor & Francis Group, Nov. 2018.

[3] C. Ma and L. Qu, "Design considerations of switched reluctance machines for structural vibration reduction," in *2017 IEEE Transportation Electrification Conference and Expo (ITEC)*, Jun. 2017, pp. 598–604.

[4] X. D. Xue, K. W. E. Cheng, and S. L. Ho, "Optimization and Evaluation of Torque-Sharing Functions for Torque Ripple Minimization in Switched Reluctance Motor Drives," *IEEE Transactions on Power Electronics*, vol. 24, no. 9, pp. 2076–2090, Sep. 2009.

[5] J. Furqani, M. Kawa, K. Kiyota, and A. Chiba, "Comparison of current waveforms for noise reduction in switched reluctance motors," in *2017 IEEE Energy Conversion Congress and Exposition (ECCE)*, Oct. 2017, pp. 752–759.

[6] A. D. Callegaro, B. Bilgin, and A. Emadi, "Radial Force Shaping for Acoustic Noise Reduction in Switched Reluctance Machines," *IEEE Transactions on Power Electronics*, pp. 1–1, 2019.

[7] S. M. Lukic and A. Emadi, "State-Switching Control Technique for Switched Reluctance Motor Drives: Theory and Implementation," *IEEE Transactions on Industrial Electronics*, vol. 57, no. 9, pp. 2932–2938, Sep. 2010.

[8] H. Makino, T. Kosaka, and N. Matsui, "Control performance comparisons among three types of instantaneous current profiling technique for sr motor," in *7th IET International Conference on Power Electronics, Machines and Drives (PEMD 2014)*, Apr. 2014, pp. 1–6.

[9] I. Manolas, G. Papafotiou, and S. N. Manias, "Sliding mode PWM for effective current control in Switched Reluctance Machine drives," in *2014 International Power Electronics Conference (IPEC-Hiroshima 2014 - ECCE ASIA)*, May 2014, pp. 1606–1612.

[10] J. Ye, P. Malysz, and A. Emadi, "A Fixed-Switching-Frequency Integral Sliding Mode Current Controller for Switched Reluctance Motor Drives," *IEEE Journal of Emerging and Selected Topics in Power Electronics*, vol. 3, no. 2, pp. 381–394, Jun. 2015.

[11] Z. Lin, D. Reay, B. Williams, and X. He, "High-performance current control for switched reluctance motors based on on-line estimated parameters," *IET Electric Power Applications*, vol. 4, no. 1, pp. 67–74, Jan. 2010.

[12] Q. Wang, H. Chen, Y. Dou, and S. Abbas, "Improved current control scheme with online current distribution and DFA regulation for switched reluctance generator," *IET Electric Power Applications*, vol. 12, no. 3, pp. 388–397, 2018.

[13] S. S. Ahmad and G. Narayanan, "Linearized Modeling of Switched Reluctance Motor for Closed-Loop Current Control," *IEEE Transactions on Industry Applications*, vol. 52, no. 4, pp. 3146–3158, Jul. 2016.

[14] J. Rodriguez and P. Cortes, *Predictive Control of Power Converters and Electrical Drives*, 1st ed. Chichester, West Sussex, UK ; Hoboken, N.J: Wiley-IEEE Press, Apr. 2012.

[15] S. Kouro, M. A. Perez, J. Rodriguez, A. M. Llor, and H. A. Young, "Model Predictive Control: MPC's Role in the Evolution of Power Electronics," *IEEE Industrial Electronics Magazine*, vol. 9, no. 4, pp. 8–21, Dec. 2015.

[16] S. S. Ahmad and G. Narayanan, "Predictive control based constant current injection scheme for characterization of switched reluctance machine," *IEEE Transactions on Industry Applications*, pp. 1–1, 2018.

[17] B. C. Torrico, R. N. d. C. Almeida, L. L. N. dos Reis, W. A. Silva, and R. S. T. Pontes, "Robust Control Based on Generalized Predictive Control Applied to Switched Reluctance Motor Current Loop," *Journal of Dynamic Systems, Measurement, and Control*, vol. 136, no. 3, Feb. 2014.

[18] R. Pupadubsin, P. Somsiri, N. Chayopitak, K. Tungpimolrut, P. Jitkreeyan, and S. Kachapornkul, "Simple predictive delta-modulation current regulator for switched reluctance motor drive," in *2008 International Conference on Electrical Machines and Systems*, Oct. 2008, pp. 3333–3337.

[19] M. Preindl and S. Bolognani, "Model Predictive Direct Torque Control With Finite Control Set for PMSM Drive Systems, Part 1: Maximum Torque Per Ampere Operation," *IEEE Transactions on Industrial Informatics*, vol. 9, no. 4, pp. 1912–1921, Nov. 2013.

[20] X. Li and P. Shamsi, "Inductance Surface Learning for Model Predictive Current Control of Switched Reluctance Motors," *IEEE Transactions on Transportation Electrification*, vol. 1, no. 3, pp. 287–297, Oct. 2015.

[21] M. Preindl and S. Bolognani, "Comparison of direct and PWM model predictive control for power electronic and drive systems," in *2013 Twenty-Eighth Annual IEEE Applied Power Electronics Conference and Exposition (APEC)*, Mar. 2013, pp. 2526–2533.

[22] M. Preindl, "Novel Model Predictive Control of a PM Synchronous Motor Drive; Design of the Innovative Structure, Feasibility and Stability Analysis, Efficient Implementation, Experimental Validation," Ph.D. Thesis, University of Padova, 2014.

[23] M. Preindl, "Robust Control Invariant Sets and Lyapunov-Based MPC for IPM Synchronous Motor Drives," vol. 63, no. 6, pp. 3925–3933.

[24] M. Preindl, E. Schaltz, and P. Thogersen, "Switching Frequency Reduction Using Model Predictive Direct Current Control for High-Power Voltage Source Inverters," *IEEE Transactions on Industrial Electronics*, vol. 58, no. 7, pp. 2826–2835, Jul. 2011.

[25] J. Ye, B. Bilgin, and A. Emadi, "An Offline Torque Sharing Function for Torque Ripple Reduction in Switched Reluctance Motor Drives," *IEEE Transactions on Energy Conversion*, vol. 30, no. 2, pp. 726–735, Jun. 2015.